

Supporting Information for

ORIGINAL ARTICLE

Intracellular aggregation of peptide-reprogrammed small molecule nanoassemblies enhances cancer chemotherapy and combinatorial immunotherapy

Jinrong Peng, Yao Xiao, Qian Yang, Qingya Liu, Yu Chen, Kun Shi, Ying Hao, Ruxia Han, Zhiyong Qian*

State Key Laboratory of Biotherapy and Cancer Center, West China Hospital, Sichuan University, and Collaborative Innovation Center of Biotherapy, Chengdu 610065, China

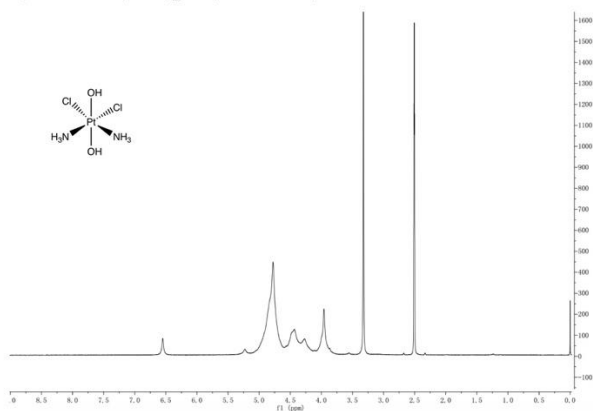
*Corresponding author.

E-mail address: anderson-qian@163.com, zhiyongqian@scu.edu.cn (Zhiyong Qian).

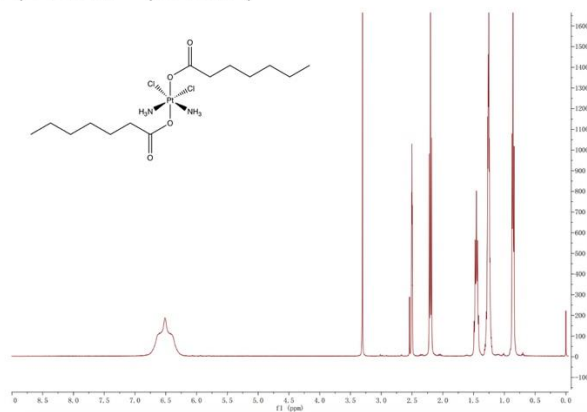
Received 5 March 2020; Received in revised form 15 April 2020; accepted 5 June 2020

Figure S1

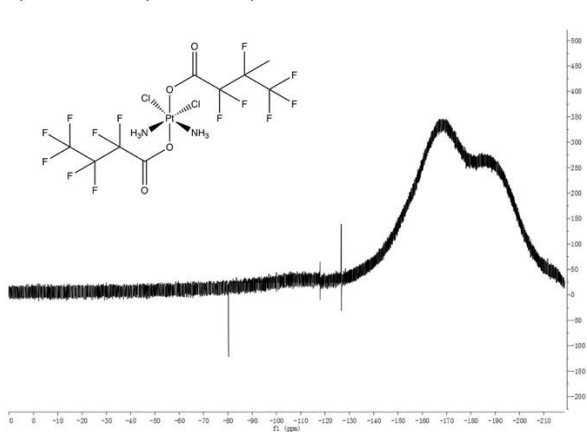
A) CDDP-(OH)₂ (¹H-NMR)



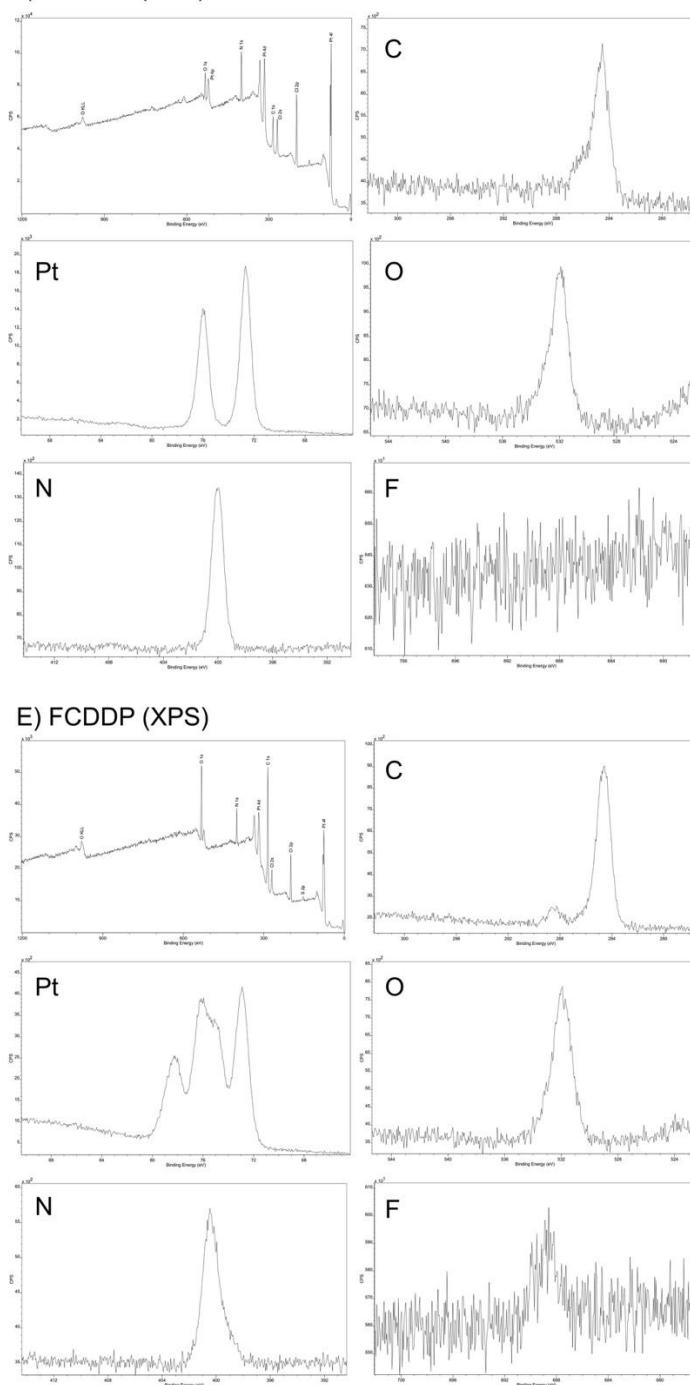
B) HCDDP (¹H-NMR)



C) FCDDP (¹⁹F-NMR)



D) HCDDP (XPS)



E) FCDDP (XPS)

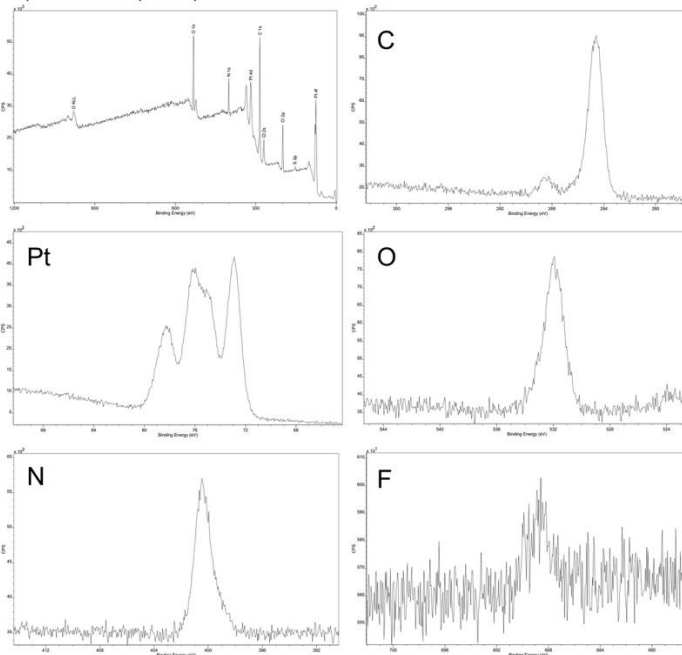


Figure S1 characterization of HCDDP and FCDDP. A) and B) are the ¹H NMR spectrum of CDDP-(OH)₂ and HCDDP, respectively. C) ¹⁹F NMR spectrum of FCDDP. D) and E) are the XPS spectrums of HCDDP and FCDDP, respectively.

Figure S2

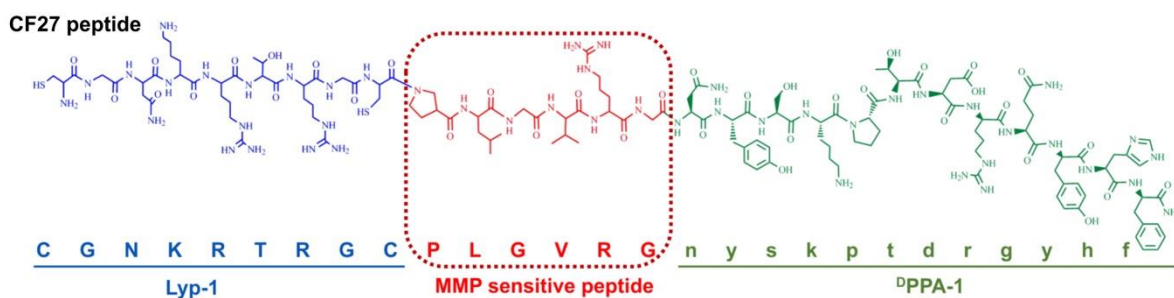


Figure S2 The chemical structure of CF27.

Figure S3

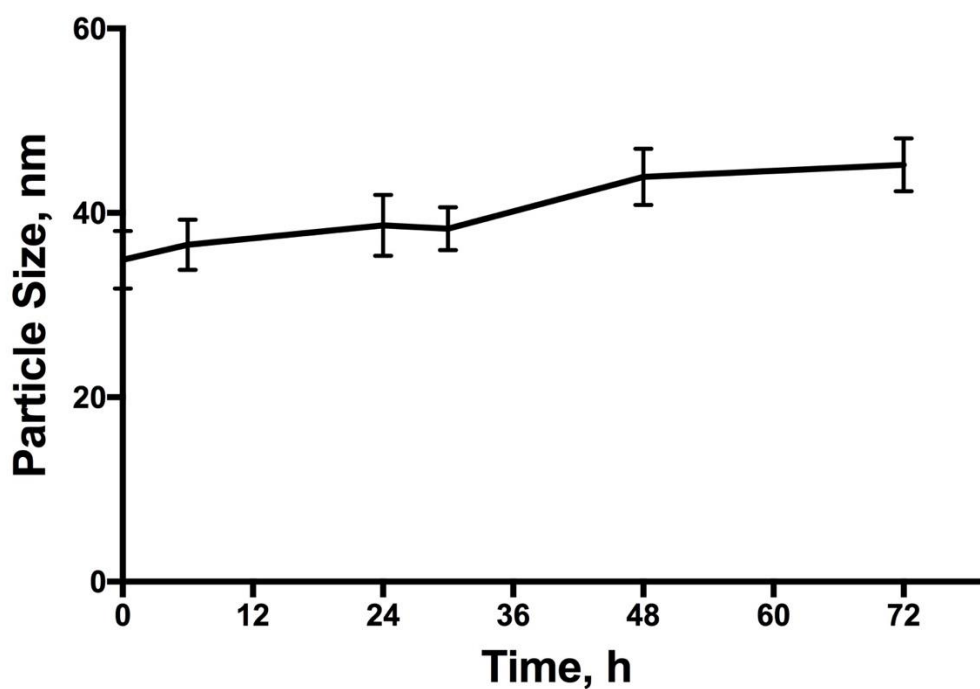


Figure S3 Stability of DFBIC in the buffer with serum. Particle size variation *versus* time. Measured by DLS. (mean \pm SD, $n=3$)

Figure S4

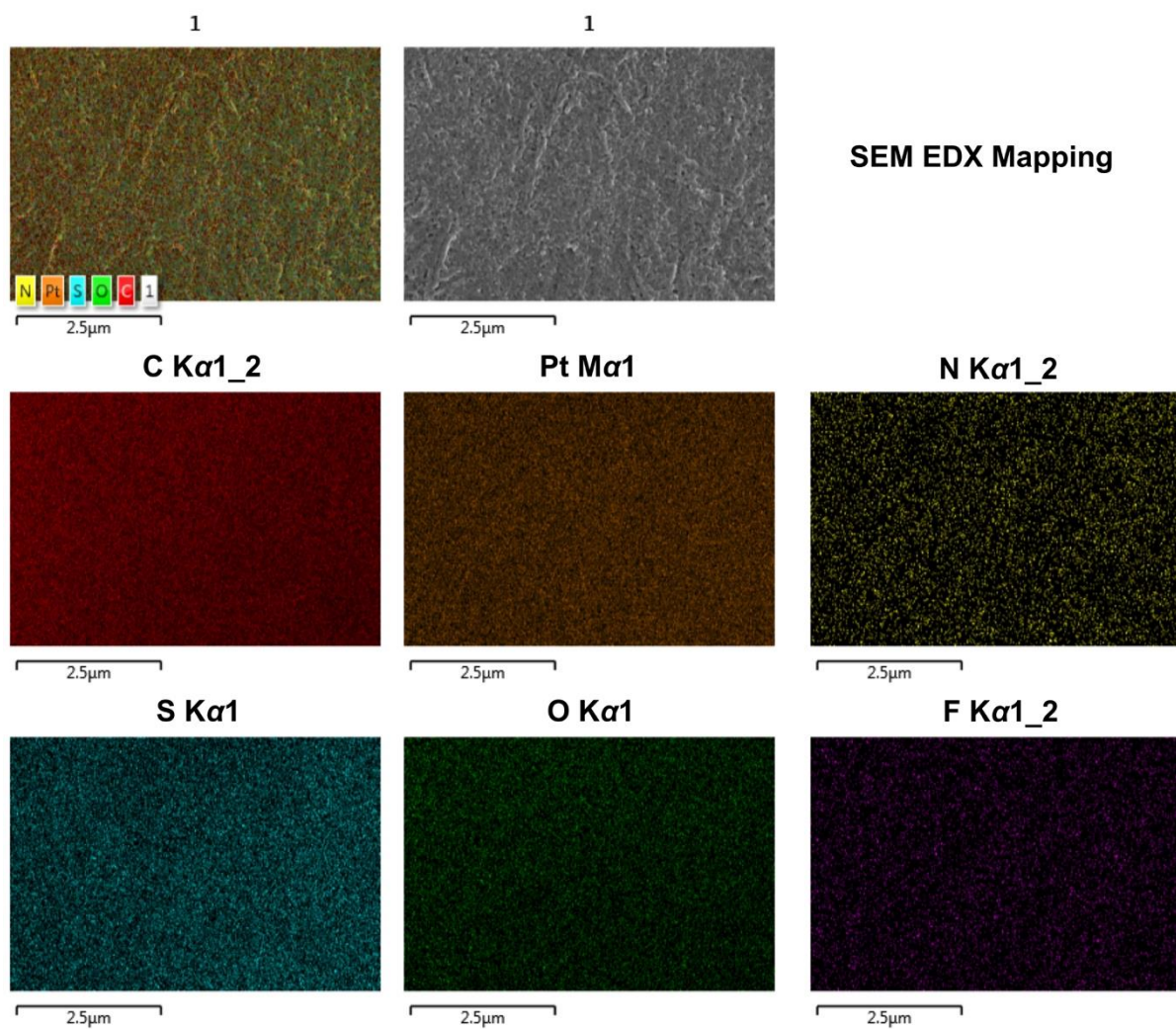


Figure S4 The EDX mapping of the nanoassemblies.

Figure S5

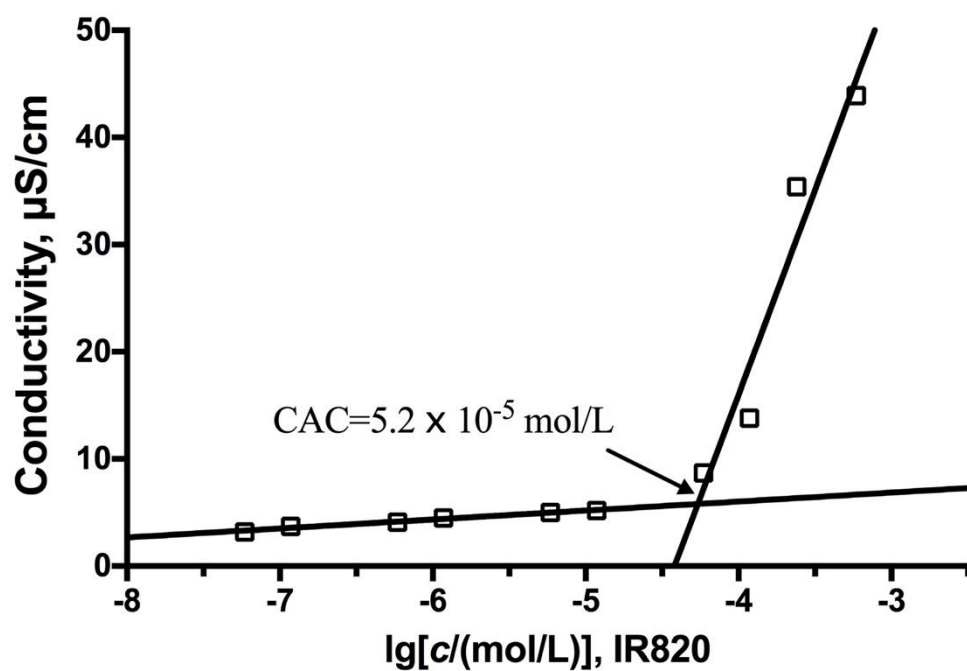


Figure S5 The critical aggregation concentration (CAC) determined by detecting the conductivity of DFBI solutions (IR820:DTX:FCDDP was 6:5:3).

Figure S6

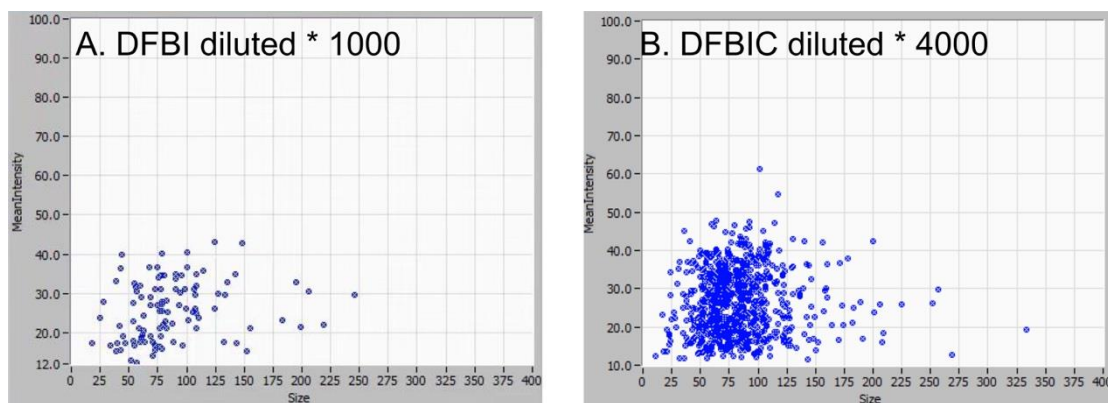


Figure S6 Particle size distribution of the nanoassemblies after dilution measured by real-time nanoparticle tracking system. The unit of the Size is nm.

Figure S7



GSH: 10

0.1 0 mM

Figure S7 No aggregation was observed in the nanoassemblies prepared without the introduction of BISS in the GSH buffers for 72 h. It indicates that the BISS is also a critical component for the formation of flocculation.

Figure S8

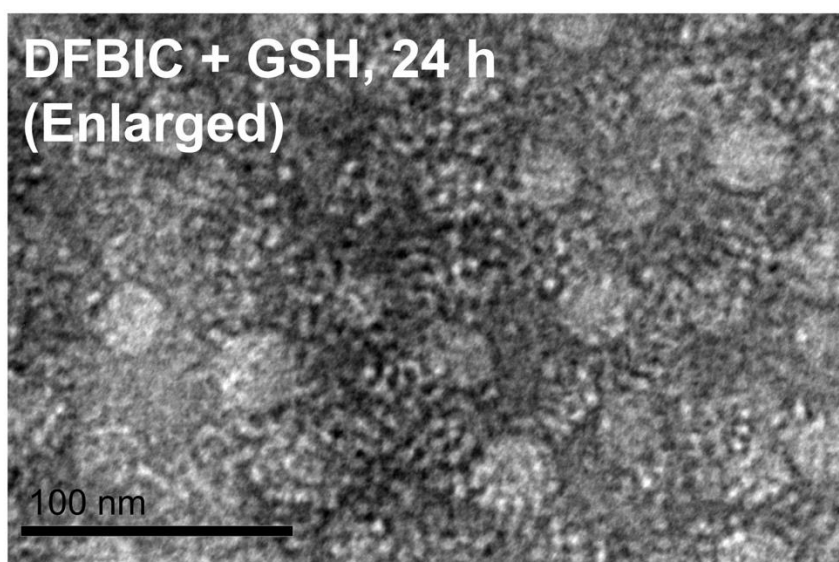
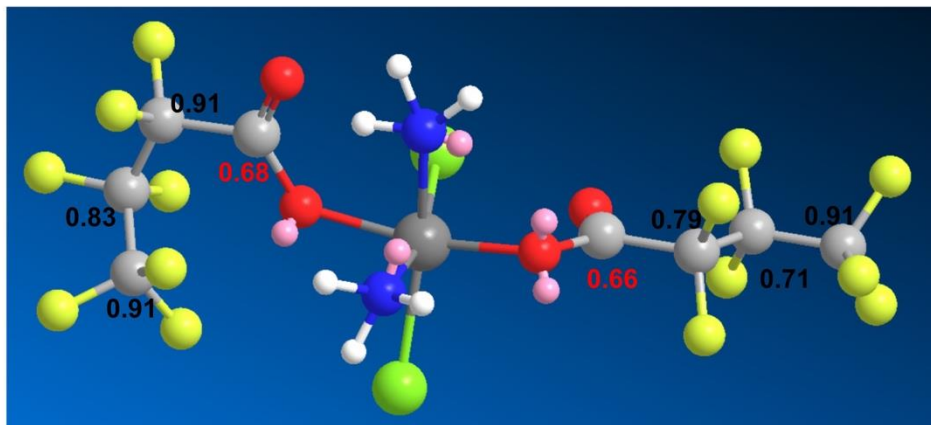


Figure S8 TEM image of nanoassemblies after treated with GSH.

Figure S9

FCDDP



HCDDP

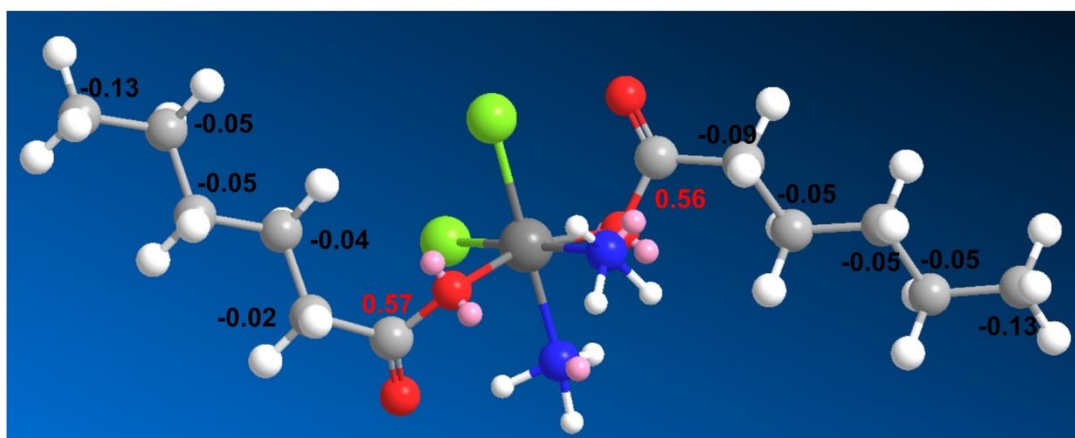


Figure S9 Charge distribution of cisplatin prodrugs.

Figure S10

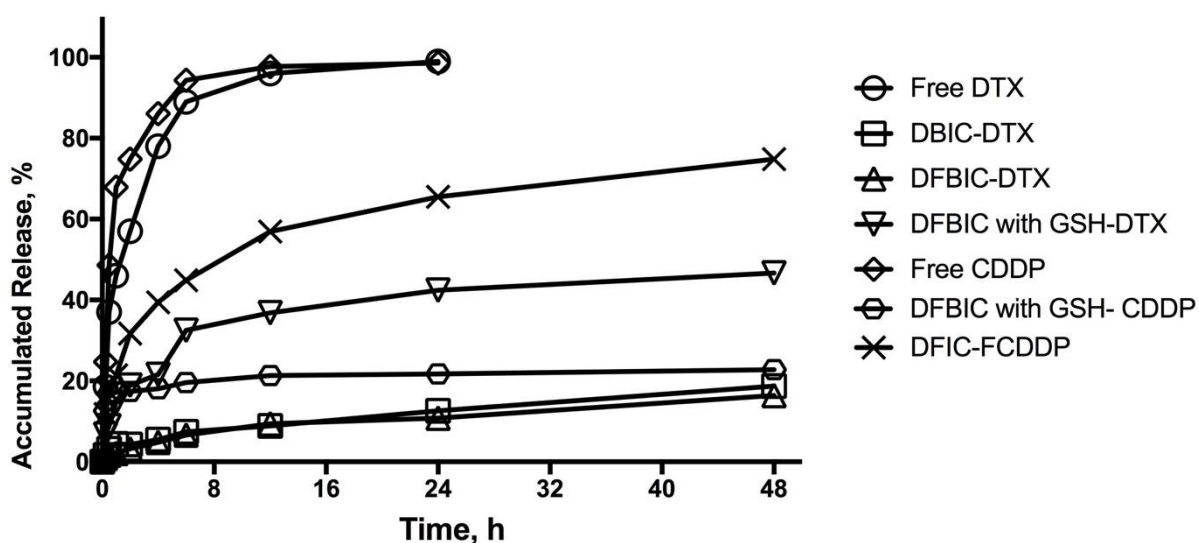


Figure S10 The release profiles of the nanoassemblies in different buffers. The parameters of the buffers: Free DTX group: pH=7.4, 0.01M PBS, 0.5% of Tween 80, GSH concentration: 0 mmol/L; DBIC-DTX group: pH=7.4, 0.01 mol/L PBS, 0.5% of Tween 80, GSH concentration: 0 mmol/L; DFBIC-DTX group: pH=7.4, 0.01M PBS, 0.5% of Tween 80, GSH concentration: 0 mmol/L; DFBIC with GSH-DTX group: pH=7.4, 0.01M PBS, 0.5% of Tween 80, GSH concentration: 10 mmol/L; Free CDDP: pH=7.4, 0.01M PBS, 0.5% of Tween 80, GSH concentration: 0 mmol/L; DFBIC with GSH-CDDP: pH=7.4, 0.01 mol/L PBS, 0.5% of Tween 80, GSH concentration: 10 mmol/L; DFIC-FCDDP: pH=7.4, 0.01 mol/L PBS, 0.5% of Tween 80, GSH concentration: 0 mmol/L.

Figure S11

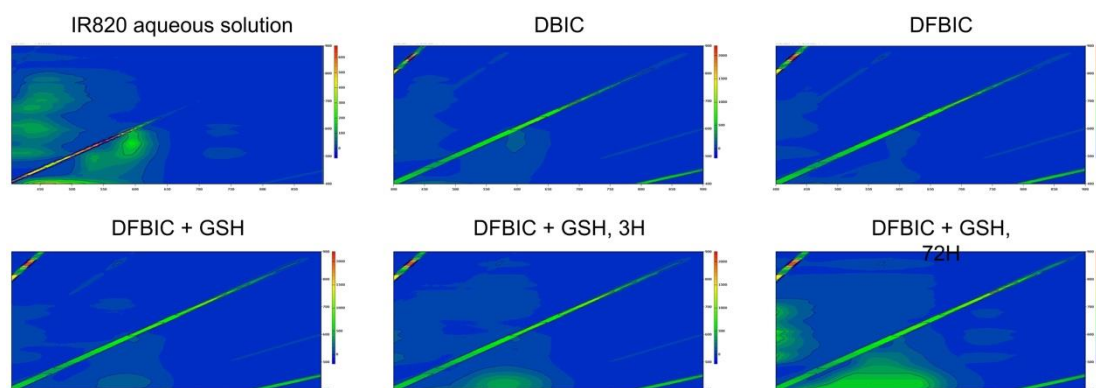


Figure S11 2D fluorescence spectra of DBIC and DFBIC with or without the presence of GSH.

Figure S12

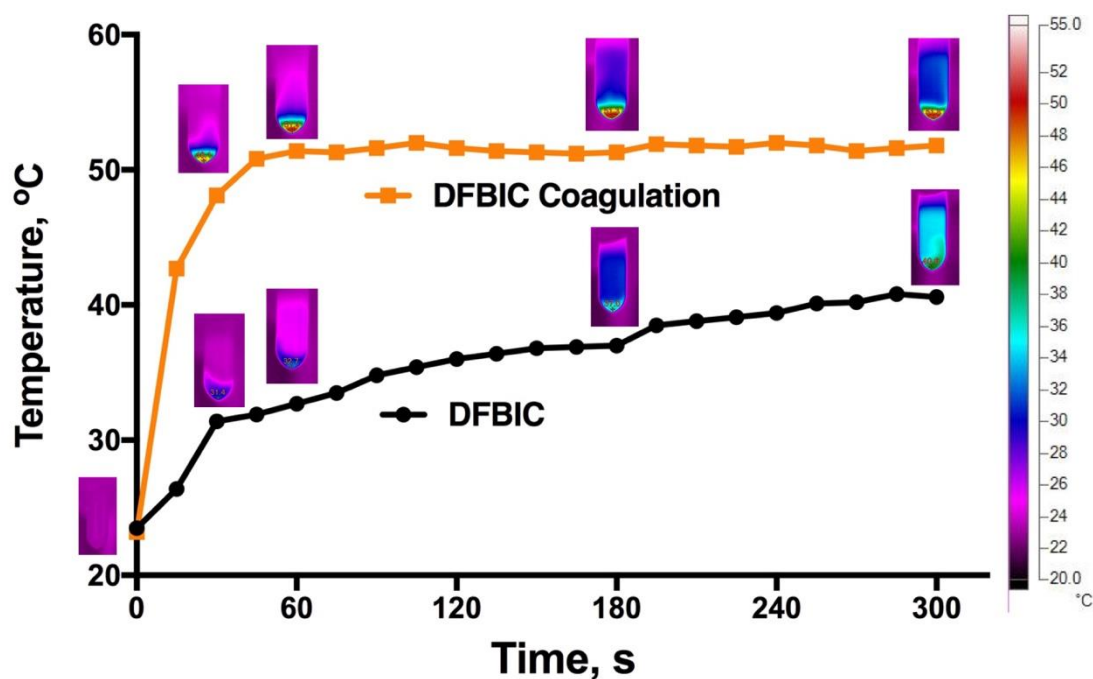


Figure S12 Photothermal conversion of DFBIC nanoassembly or the coagulation of DFBIC.

Figure S13

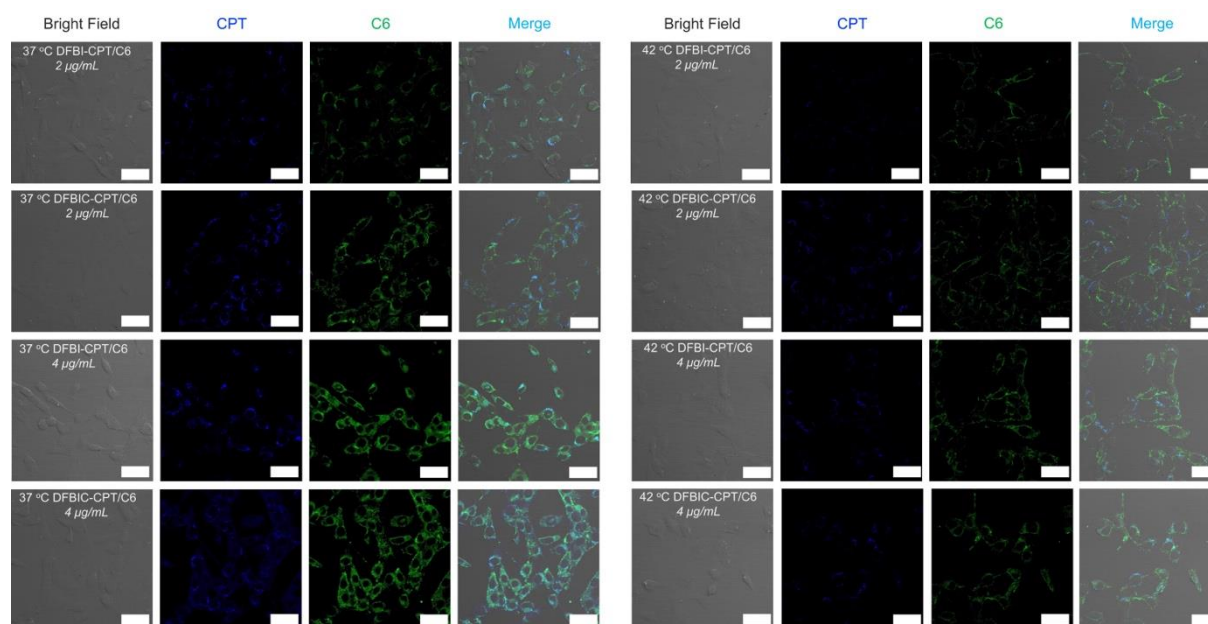


Figure S13 Intracellular aggregation of nanoassemblies (DFBIC and DFBI) *in vitro*. Left: The cancer cells were treated with two different concentration (2 and 4 $\mu\text{g/mL}$, respectively) of two different nanoassemblies (DFBIC and DFBI, respectively). Right: The cancer cells were treated with mild heating while treating with two different concentration (2 and 4 $\mu\text{g/mL}$, respectively) of two different nanoassemblies (DFBIC and DFBI, respectively). Scale bar = 40 μm .

Figure S14

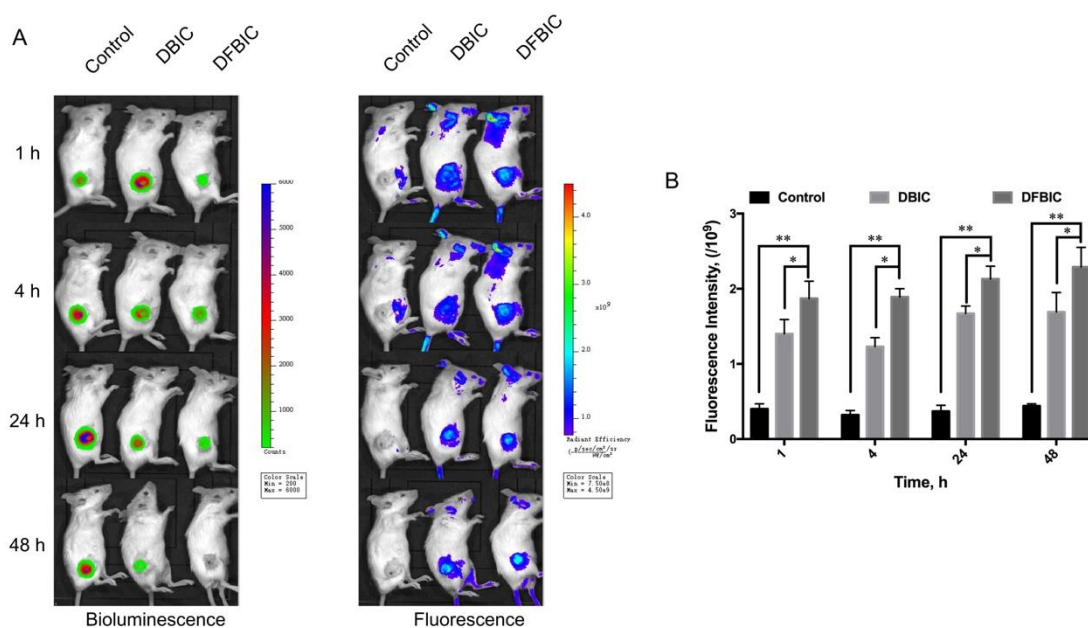


Figure S14 Tumor-targeting ability of nanoassemblies. A) Living fluorescence images of the mice treated with different nanoassemblies. B) Fluorescent intensity of the tumors. (mean \pm SD, $n=3$, * $P < 0.05$, ** $P < 0.01$).

Figure S15

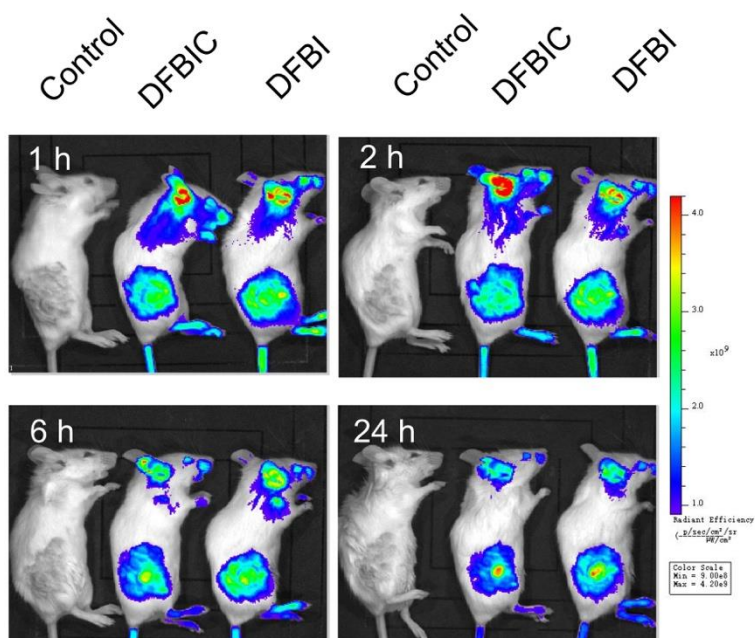


Figure S15 Effect of modification of the tumor-targeting ligand onto the accumulation of nanoassemblies in the tumor site.

Figure S16

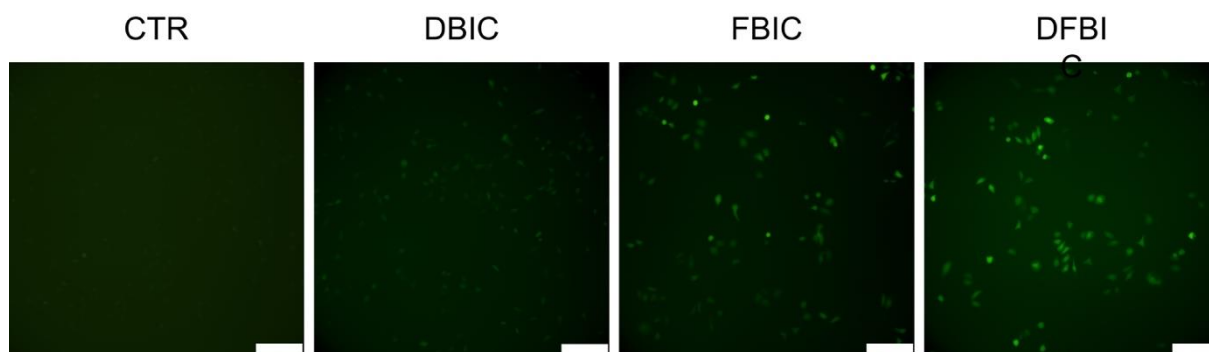


Figure S16 The ROS production of the MDA-MB-231 cell lines after incubated with control, DBIC, FBIC, DFBI, respectively. The fluorescent images of the tumor cells, 2.5 $\mu\text{g}/\text{mL}$ (DTX). Scale bar = 100 μm .

Figure S17

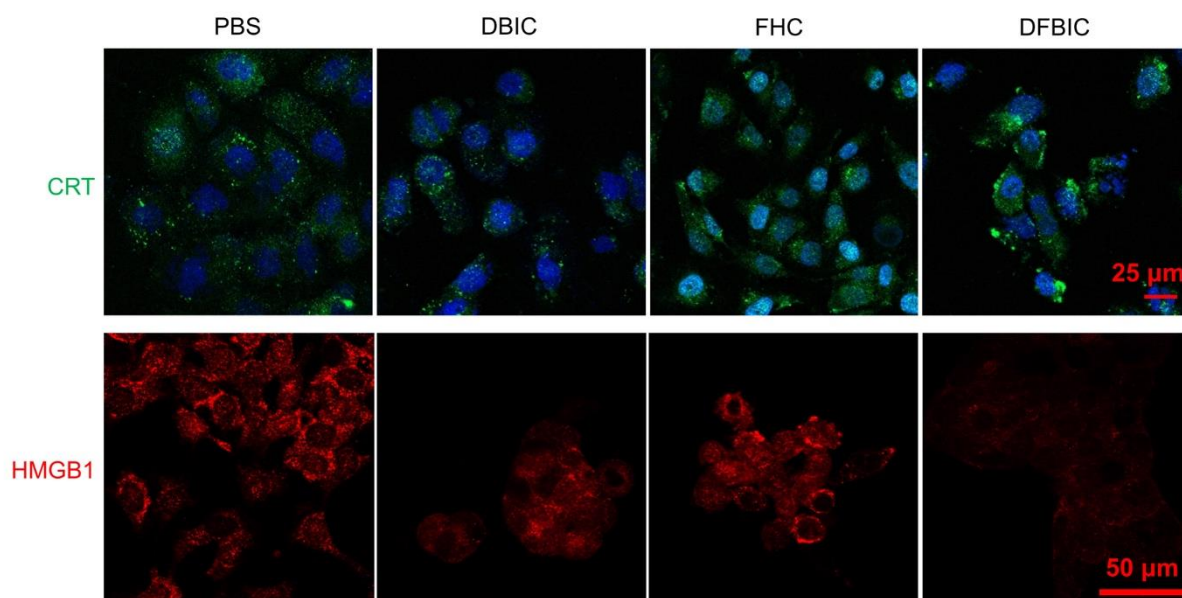
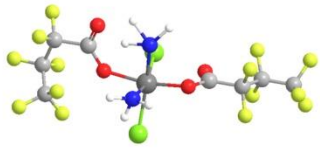


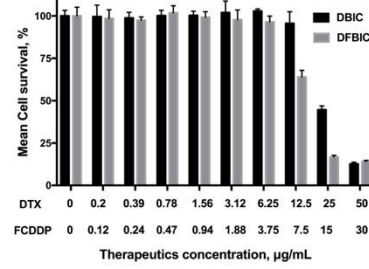
Figure S17 The migration of CRT and HMGB1 *in vitro* after being treated with nanoassemblies.

Figure S18

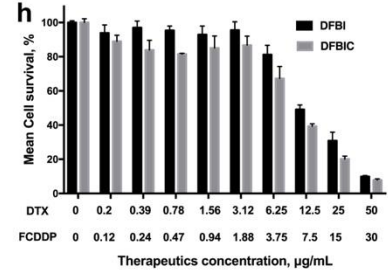
A1



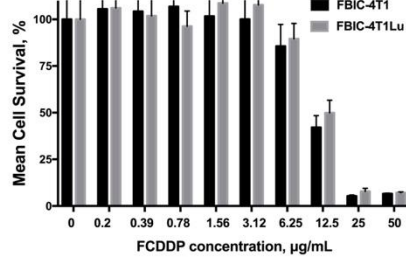
231-24 h



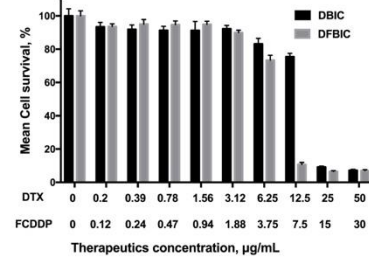
231-24 h



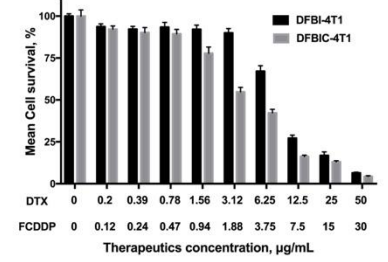
4T1-24 h



231-48 h

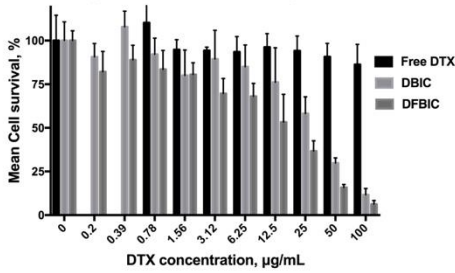


4T1-24 h

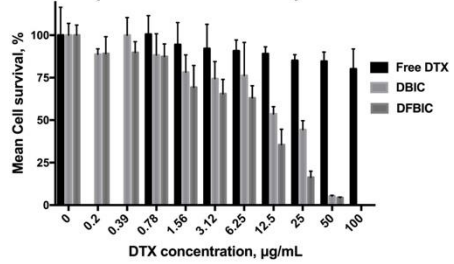


A2

HCT8 (PTX resistance)-24 h



HCT8 (PTX resistance)-48 h



C

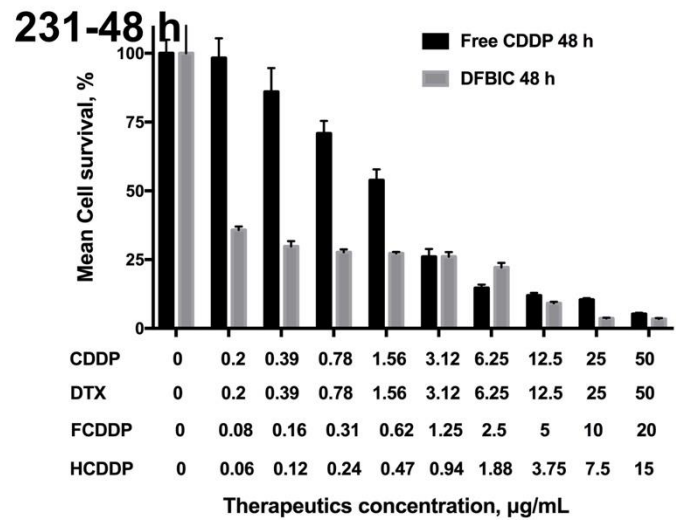
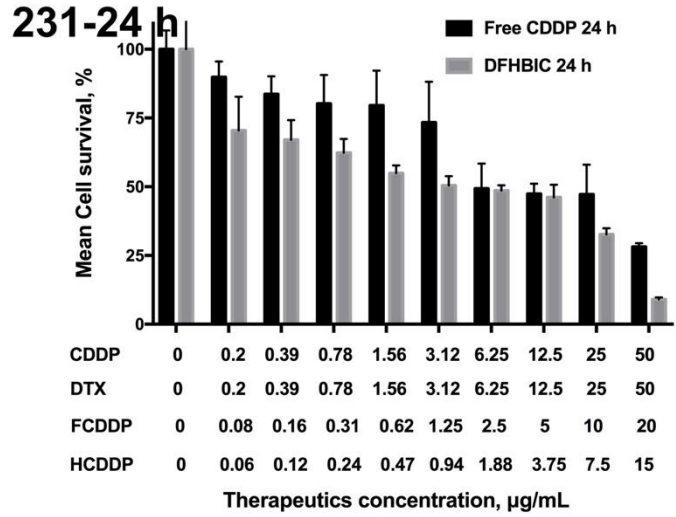
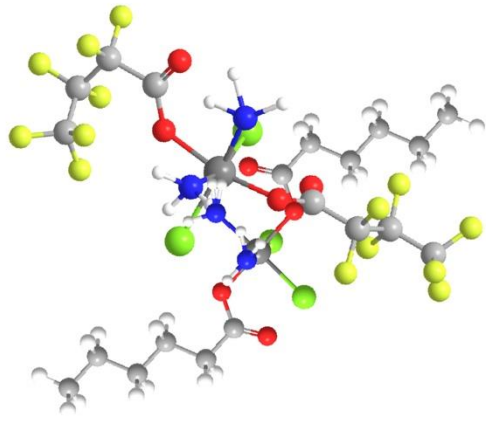


Figure S18 Cytotoxicity of nanoassemblies to different cancer cell lines. (mean \pm SD, $n=6$). (A) the cytotoxicity of DFBIC to different cancer cell lines (including a PTX resistant cell line). (B) the cytotoxicity of DHBIC to different cancer cell lines. (C) the cytotoxicity of DFHBIC to different cancer cell lines.

Figure S19

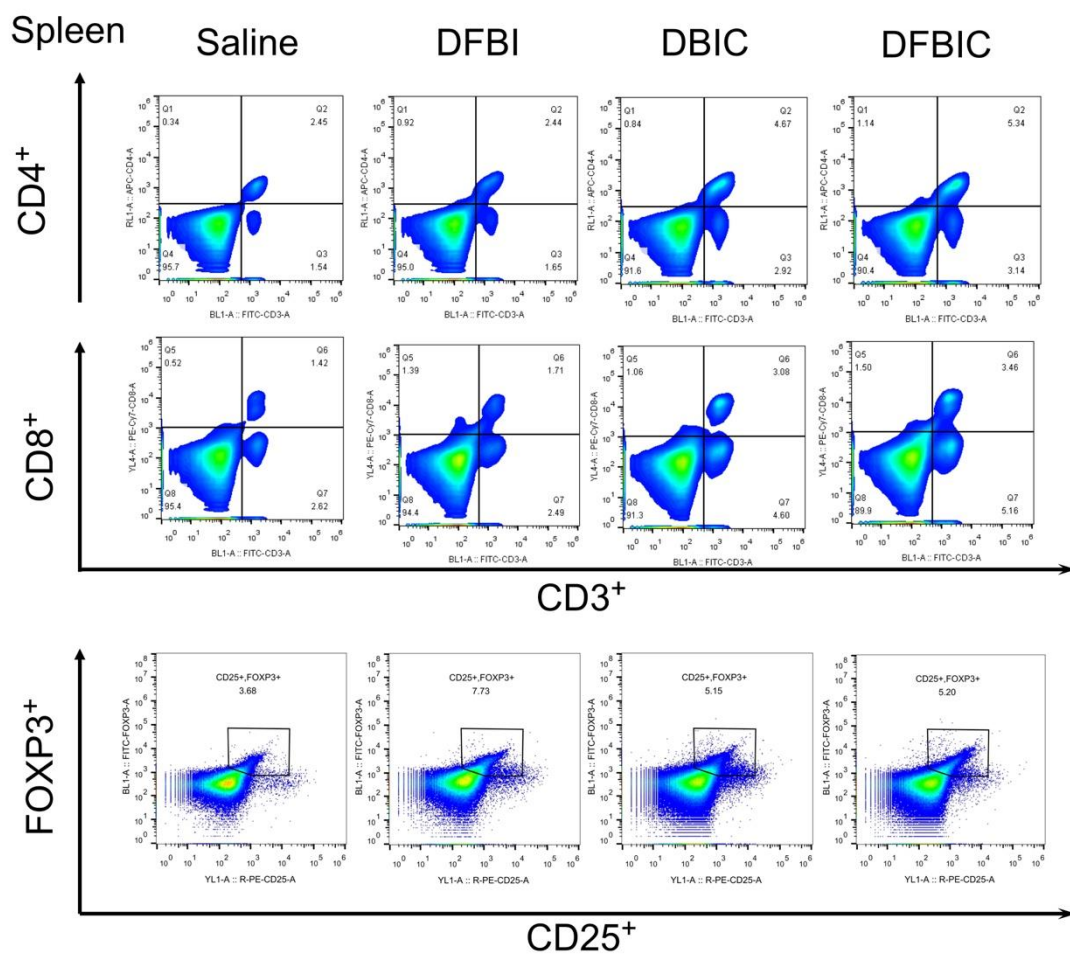


Figure S19 Polulation of different immunocytes which extracted from the spleen tissues after being treated with different nanoassemblies and identified by flow cytometry.

Figure S20

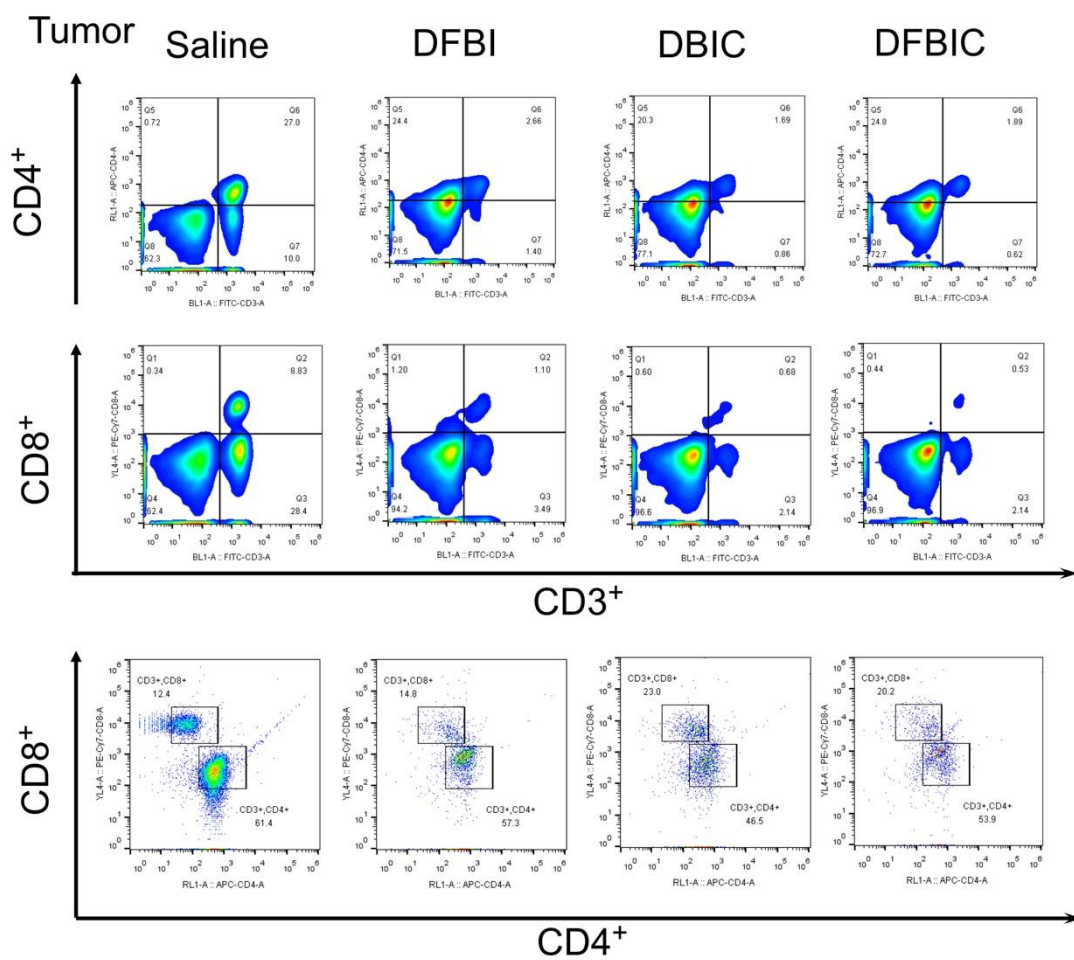


Figure S20 Polulation of different immunocytes which extracted from the tumor tissues after being treated with different nanoassemblies.

Figure S21

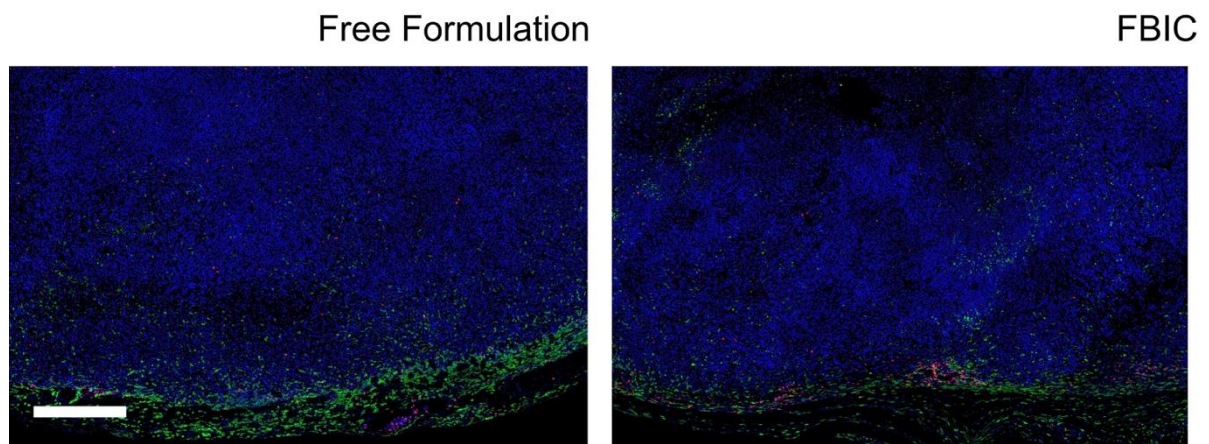


Figure S21 Immunofluorescent staining of tumor tissues slide which extracted from the free formulation and FBIC-treated groups. Tumor tissues were all co-stained with DAPI, α CD8 and α IFN- γ . Scale bar = 500 μ m.